

## Article

# On the Influence of the Microstructure upon the Fatigue and Corrosion Fatigue Behavior of UNS N07718

Christopher Tom Engler <sup>1,\*</sup>, Helmuth Sarmiento Klapper <sup>2</sup> and Matthias Oechsner <sup>1</sup>

<sup>1</sup> Center for Structural Materials (MPA-IfW), Grafenstraße 2, 64283 Darmstadt, Germany; oechsner@mpa-ifw.tu-darmstadt.de

<sup>2</sup> Baker Hughes, Baker-Hughes-Straße 1, 29221 Celle, Germany; helmuth.sarmiento-klapper@bakerhughes.com

\* Correspondence: engler@mpa-ifw.tu-darmstadt.de; Tel.: +49-6151-16-25070

**Abstract:** Due to the challenging operational conditions occurring during drilling, e.g., in the oil and gas industry, the corrosion fatigue (CF) behavior of materials used in drillstring components needs to be well understood. The combination of cyclic mechanic loads and a corrosive environment can affect significantly the integrity of a material, which has to be taken into account when selecting and qualifying materials for drilling equipment. Nickel alloys such as the precipitation-hardenable alloy 718 (UNS N07718) are widely used in many industrial applications including subterranean drilling. In the present study, the fatigue and CF behavior of alloy 718 in three different metallurgical conditions was investigated. The CF behavior of the different conditions was determined using customized rotating bending machines enabling testing in a simulated drilling environment at 125 °C. Results have shown that the fatigue and CF strength of alloy 718 is affected by its microstructural particularities, for instance, the amount of strengthening phases and  $\delta$ -phase.

**Keywords:** fatigue; corrosion fatigue (CF); pitting corrosion; alloy 718 (UNS N07718); oil and gas; drilling technology



**Citation:** Engler, C.T.; Klapper, H.S.; Oechsner, M. On the Influence of the Microstructure upon the Fatigue and Corrosion Fatigue Behavior of UNS N07718. *Metals* **2021**, *11*, 117. <https://doi.org/10.3390/met11010117>

Received: 21 December 2020

Accepted: 7 January 2021

Published: 9 January 2021

**Publisher's Note:** MDPI stays neutral with regard to jurisdictional claims in published maps and institutional affiliations.



**Copyright:** © 2021 by the authors. Licensee MDPI, Basel, Switzerland. This article is an open access article distributed under the terms and conditions of the Creative Commons Attribution (CC BY) license (<https://creativecommons.org/licenses/by/4.0/>).

## 1. Introduction

The mechanical fatigue of engineering materials has been extensively investigated. On the other hand, corrosion fatigue (CF) behavior and the mechanisms that rule CF have been less studied. This is quite surprising because CF is one of the most important environmentally-assisted cracking (EAC) mechanisms affecting components subjected to cyclic loading in a corrosive environment. Indeed, CF is an important limiting factor in the lifetime of these components in service. The fact that CF has received less attention can be partially explained by the difficulty in simulating accurately cyclic loading conditions and corrosive environments. This is particularly true at elevated temperatures, which are usually present in many industrial applications where CF becomes relevant. Subterranean drilling, for instance in oil and gas (O&G) exploration, is one of these applications. During directional drilling operations, structural materials in the drillstring are subjected, among other types of mechanical loads, to fully reverse bending moments while in permanent contact with the drilling fluid, which is usually a mixture of bentonite clay with fresh water and some polymer additives [1]. Water-based drilling fluids might also include large amounts of chloride ( $\text{Cl}^-$ )-ions. Drilling fluids can be saturated with salts, sometimes to adjust some properties in the fluid, sometimes due to pick-up from the geological formation. High Cl-concentrations increase the susceptibility to localized corrosion of metallic materials used in the drillstring. The addition of alkaline compounds such as calcium or sodium hydroxide to the drilling fluid constitutes the traditional method for providing corrosion protection by maintaining the pH of the drilling fluid in the alkaline region [2]. However, service temperatures well beyond 100 °C are common in deep wells creating a very corrosive environment, which in combination with cyclic loading increases significantly the likelihood of CF on metallic materials used in drillstring components.

Indeed, CF has been identified as one of the most common causes of failure in downhole drilling equipment [1]. The widespread use of directional drilling has increased the importance of CF strength in materials selection for drilling equipment. On the one hand, the chemical composition, pH and oxygen content of the drilling fluid as well as temperature need to be considered. On the other hand, the mechanical loads acting on the components, the material properties and the time the drillstring is subjected to these conditions also play a crucial role. Therefore, a good understanding about the susceptibility of structural materials used in the drillstring to CF should take into account all these factors.

The precipitation-hardenable nickel iron chromium alloy 718 (UNS N07718) was originally developed for use in power generation [3]. The exceptional combination of high strength, thermal stability, and excellent corrosion resistance has led to its successful application in other industrial sectors including O&G [3–8], aerospace [9,10] and military applications [11]. The chemical, microstructural and mechanical properties of alloy 718 for O&G applications are specified in API standard 6ACRA [12], where three different yield strength levels ranging between 827 and 1034 MPa are defined. The austenitic matrix in alloy 718 is strengthened by the intermetallic precipitates  $\gamma'$  ( $L_{12}$  structure,  $Ni_3(Al,Ti)$ ) and  $\gamma''$  ( $DO_{22}$  structure,  $Ni_3Nb$ ) produced by precipitation hardening. The amount and shape of these precipitates depends predominantly upon the hardening temperature and time used to establish the desired strength in the material [13]. In addition, these microstructural particularities play also a role on the cracking resistance of alloy 718 [14,15]. Alloy 718 in solution annealed and age hardened condition to yield strengths beyond 964 MPa is commonly used in components for state-of-the-art drilling technologies due to its uniform mechanical properties, adequate non-magnetic character, thermal stability, and superior corrosion resistance when compared to other metallic materials used in drilling equipment, typically austenitic CrMn stainless steels [8,10,16].

In spite of the extensive data available on the corrosion resistance of alloy 718, its CF behavior remains unrevealed, especially in hot brines at elevated temperatures. In this research work, CF tests have been conducted to assess the resistance of alloy 718 in solution annealed and precipitation hardened condition to fatigue in an alkaline brine at 125 °C that simulates a typical drilling environment. In addition, fatigue and electrochemical examinations were conducted to determine the influence of fatigue strength and pitting susceptibility on the observed CF behavior of the material.

## 2. Materials and Methods

Specimens were taken from commercial bar stock of alloy 718 with diameters ranging between 127 up to 203 mm. In all cases the manufacturing route as well as the chemical composition of the material met the requirements of API Standard 6ACRA [12] for UNS N07718. The chemical composition, that was measured using optical emission spectroscopy (OES) of one of the investigated materials is included in Table 1 for reference.

**Table 1.** Chemical composition in wt % of one of the investigated materials measured using optical emission spectroscopy (OES).

| Cr   | Mo  | Ni   | Al   | Nb  | Ti   | Mn   | Fe   | Rest |
|------|-----|------|------|-----|------|------|------|------|
| 18.6 | 3.0 | 53.7 | 0.45 | 5.0 | 0.83 | 0.08 | 17.3 | 1.04 |

In this study, alloy 718 was investigated in three different metallurgical conditions. All materials were in a solution annealed and precipitation-hardened condition. While the solution annealing step was in all cases at 1030 °C, above the  $\delta$ -solvus temperature, followed by water quenching. Subsequently, three precipitation hardening treatments were used to produce different strength levels. Condition 1 corresponds to a single age-hardening step at 780 °C for 8 h. Material in condition 1 is expected to have a minimum yield strength of 965 MPa [12], and a microstructure characterized by a  $\gamma'/\gamma''$ -ratio of 0.92 as well as limited amount of  $\delta$ -phase at the grain boundaries [15]. The second and

third conditions correspond to double aging treatments commonly used for aerospace applications. These treatments lead to a refinement of the strengthening phases and avoid almost completely  $\delta$ -phase formation. To reach condition 2, the material in the solution annealed condition was initially hold for 8 h at a temperature close 720 °C, followed by 8 h after cooling to approx. 620 °C. This heat treatment produces a  $\gamma'/\gamma''$ -ratio of 1.36 [15]. The two age-hardening steps used for condition 3 involved slightly higher temperatures and shorter ageing times. Alloy 718 in conditions 2 and 3 is expected to exhibit higher yield strength compared to condition 1, typically above 1035 MPa.

### 2.1. Fatigue and Corrosion Fatigue Tests

Fatigue and CF examinations were conducted under constant stress amplitude ( $S_a$ ) at stress ratio  $R = -1$  using a customized 4-point rotating bending machine, which simulates closely the loading scenario experienced during drilling applications, Figure 1.



**Figure 1.** Test setup including a 4-point rotating bending machine with external heating device.

The specimen was rotated at 3000 rpm (50 Hz), and the applied load was controlled by a calibrated load cell. Fatigue tests were conducted in air at room temperature (RT) while CF tests were performed in a buffer NaCl/KCl-solution with a  $\text{Cl}^-$ -content of 2.25 mol/L and a pH of 9 at 125 °C set by 0.032 mol/L of NaOH. The solution was contained in a chamber made of Ti6Al4V-alloy (UNS R56400). The temperature in the test chamber was continuously monitored and controlled by a thermocouple located directly inside the chamber, therefore, in contact with the test solution, and an external heating device surrounding the chamber (Figure 1). In order to conduct CF tests at elevated temperatures a customized design was required to enable the temperature-induced expansion of the specimens and prevent additional undesired loads. This was achieved by implementing a mounting device that is able move freely in axial direction. In addition, 4-point bending mode was chosen because it results in a more homogenous load distribution at the gauge area simultaneously exposed to the electrolyte. This is a clear improvement compared to the typical punctiform load achieved by 2-point bending. In addition, the desired test area can be determined by adjusting the specimen geometry. This has a beneficial impact when testing under corrosive conditions as a larger area of the specimen will be subjected to the same corrosive and loading conditions [17]. The applied load ( $S_a$ ) was varied from specimen to specimen and a run-out was established at  $2 \times 10^7$  cycles.

### 2.2. Electrochemical Tests

The susceptibility to pitting corrosion of alloy 718 in the three different metallurgical conditions was determined by open-circuit potential (OCP) and cyclic potentiodynamic polarization measurements using a 3-electrode arrangement in an autoclave. The test

solution was identical to the one used in the CF-tests (2.25 mol/L  $\text{Cl}^-$  solution of pH 9 at 125 °C). L-shaped specimens were taken by wire-electrical discharge machining (EDM) in longitudinal direction and used as working electrodes. The longest portion of the specimen is used for electrical contact while the rest of the surface (845 mm<sup>2</sup>) is in contact with the electrolyte, thus avoiding crevice corrosion or selective corrosion at the wire that typically occurs during testing at elevated temperatures on embedded or spot-welded specimens. The specimen was positioned in the electrochemical cell screwing it to a specimen holder manufactured using Ti6Al4V-alloy. An external 3 M KCl/Ag/AgCl reference electrode (207 mV<sub>SHE</sub>) suitable for high temperature applications and a Ti-oxide covered Ti-mesh were used as reference and counter electrodes, respectively.

Prior to the electrochemical measurements, each specimen was mechanically grinded to grit 360 using SiC-paper. Subsequently, it was rinsed with deionized water and ethanol, and dried with air. After drying the specimen was immediately immersed into a fresh prepared test solution (approx. 500 mL), which was previously purged 30 min with pure nitrogen (99.999% N<sub>2</sub>) to remove traces from atmospheric oxygen. The OCP was then measured over a period of two hours. The first hour corresponds to the period of time necessary for the solution to reach the testing temperature. During the second hour the OCP was measured at a constant temperature of 125 °C. The polarization scan was started at −100 mV from the OCP measured after two hours of immersion in the test solution. The scan was initially conducted in anodic direction using a scan rate of 0.2 mV/s. After reaching a current density of 10<sup>−4</sup> A/cm<sup>2</sup> the polarization was switched in the cathodic direction. The threshold of 10<sup>−4</sup> A/cm<sup>2</sup> was also used for defining the pitting potential ( $E_{\text{pit}}$ ) during the polarization scan in the anodic direction. The repassivation potential ( $E_{\text{rp}}$ ) was established as the potential necessary for the current density to return to a value of 10<sup>−4</sup> A/cm<sup>2</sup> during the cathodic polarization scan. The selection of these experimental parameters is based on preliminary results discussed elsewhere [18]. The corrosion potential ( $E_{\text{corr}}$ ) was taken from the potentiodynamic plots at the lowest current density. Electrochemical tests were conducted at least three times to assess the reproducibility of the results.

### 3. Results

#### 3.1. Pitting Susceptibility

Typical cyclic potentiodynamic polarization curves obtained on alloy 718 in the alkaline brine at 125 °C are included in Figure 2. The electrochemical behavior of all three different material conditions in the test environment was very similar and characterized by a long passive region and excellent pitting corrosion resistance. No statistically significant difference was observed between the different conditions. A peak in the current density was reproducibly observed within the passive region during the anodic polarization scan. At a potential around 300 mV<sub>SHE</sub> the current density increased to approx. 10<sup>−5</sup> A/cm<sup>2</sup> for all the conditions. Rather than localized corrosion, it is assumed that this peak relates to the stabilization of the passive layer formed on alloy 718 in the alkaline testing solution at 125 °C. After this initial current density increase, the current density dropped slightly before it rapidly increased again at polarization potentials more noble than 400 mV<sub>SHE</sub>. No metastable pitting activity was observed during the anodic polarization scan before stable pit growth occur, which was characterized by a rapid increase in the current density to values beyond 5 × 10<sup>−4</sup> A/cm<sup>2</sup>. The current density only dropped to values below 10<sup>−5</sup> A/cm<sup>2</sup> at polarization potentials around 70 mV<sub>SHE</sub> during the cathodic polarization scan. This drop in the current density indicates the repassivation of the surface. Table 2 summarizes the electrochemical parameters obtained from the OCP and polarization measurements. As shown in the polarization curves as well as in the values included in Table 2, no statistically significant difference was determined among the electrochemical parameters determined for all three metallurgical conditions.

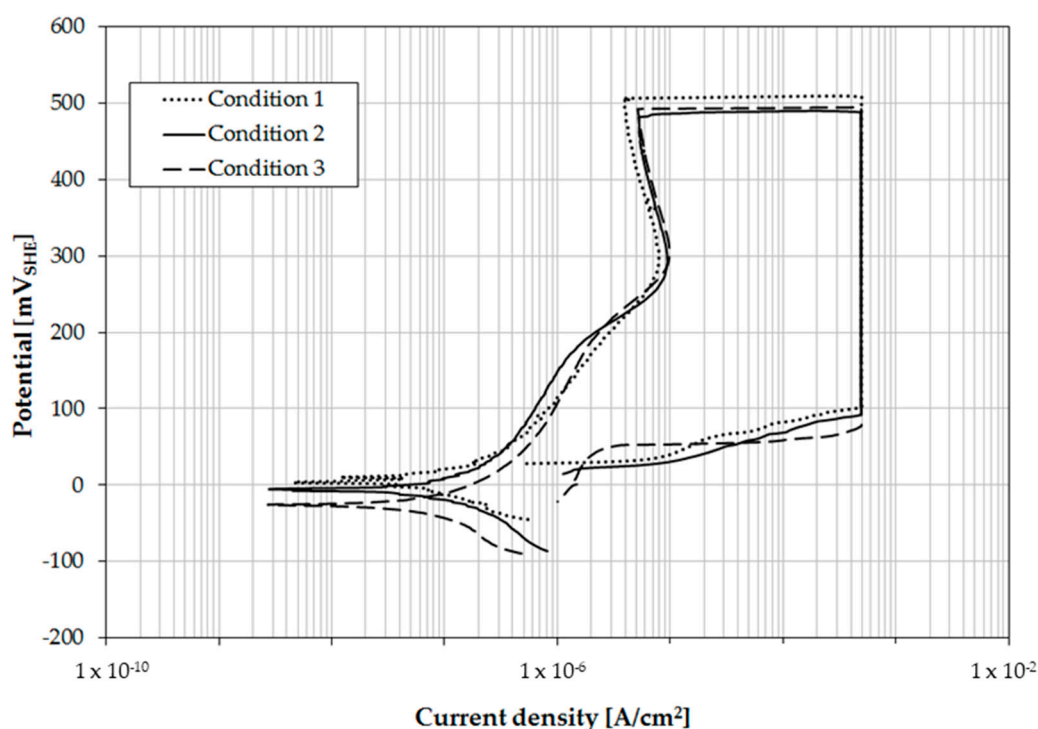


**Figure 2.** Typical cyclic polarization curves of alloy 718 in 2.25 mol/L  $\text{Cl}^-$ -sol. of pH 9 at 125 °C.

**Table 2.** Electrochemical parameters of alloy 718 in 2.25 mol/L  $\text{Cl}^-$ -sol. of pH 9 at 125 °C.

| Condition | OCP<br>(mV <sub>SHE</sub> ) | E <sub>corr</sub><br>(mV <sub>SHE</sub> ) | E <sub>pit</sub><br>(mV <sub>SHE</sub> ) | E <sub>rp</sub><br>(mV <sub>SHE</sub> ) |
|-----------|-----------------------------|---|--|---|
| 1         | 18 ± 32                     | −46 ± 50                                  | 508 ± 21                                 | 61 ± 20                                 |
| 2         | −62 ± 28                    | −53 ± 50                                  | 460 ± 68                                 | 86 ± 24                                 |
| 3         | 25 ± 13                     | −15 ± 10                                  | 440 ± 69                                 | 68 ± 10                                 |

### 3.2. Results of Corrosion Fatigue Tests

As indicated previously, rotating-bending tests were performed on all three material conditions in air at room temperature and in a buffer of NaCl/KCl-solution with a pH of 9 at 125 °C. The results are presented in Figure 3 in form of S/N curves that were calculated using a survival probability of 50%. Runouts are designated in Figure 3 by arrows pointing towards higher cycles to failure. As shown in Figure 3, condition 3, which owns the highest tensile strength, exhibits the longer lifetimes and highest fatigue strength among all conditions, regardless the test environment. A similar slope of the S/N curves ( $k$ ) was obtained for conditions 2 and 3, 9 and 10, respectively. It is also remarkable, that condition 1 having the lowest strength has shown a fatigue behavior (in air at room temperature) similar to condition 3, which is confirmed by the obtained runouts (Figure 3).

The fatigue strength of condition 3 in the brine at 125 °C was reduced to the one obtained by condition 2 in air at room temperature. In addition, no environmental influence was determined on the fatigue behavior of condition 2. This suggests an excellent resistance of this metallurgical condition to corrosion also in the presence of cyclic mechanical loads. The scatter of the data for condition 2 is more pronounced in the very-high-cycle-fatigue (VHCF) region, though (Figure 4). This indicates a transition to stress amplitudes with higher lifetimes. First runouts for condition 2 were obtained at stress amplitudes almost 50 MPa higher compared to those for condition 3. On the other hand, the CF strength of condition 1 is slightly lower compared to condition 2 and 3. However, this condition experiences the largest reduction in fatigue strength when exposed to the brine at 125 °C.



At this point, it has to be mentioned that none of the alloy 718 specimens have shown signs of localized corrosion after the CF tests by visual inspection.

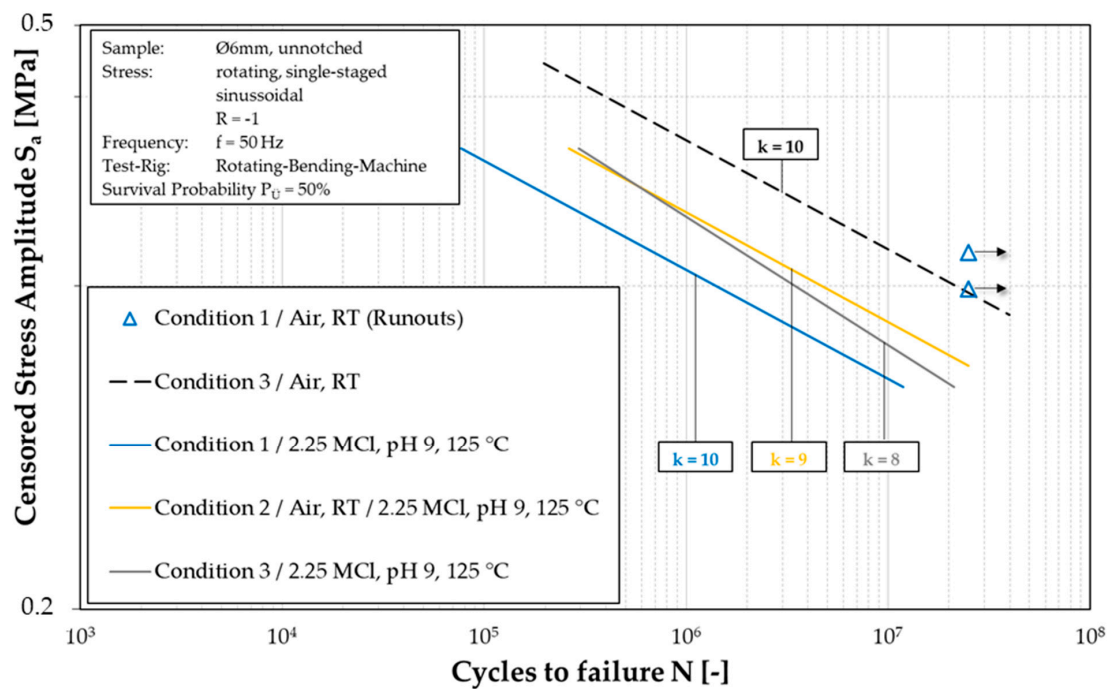


**Figure 3.** Results of fatigue and CF tests on alloy 718 represented using double logarithmic S/N curves (survival probability of 50%).

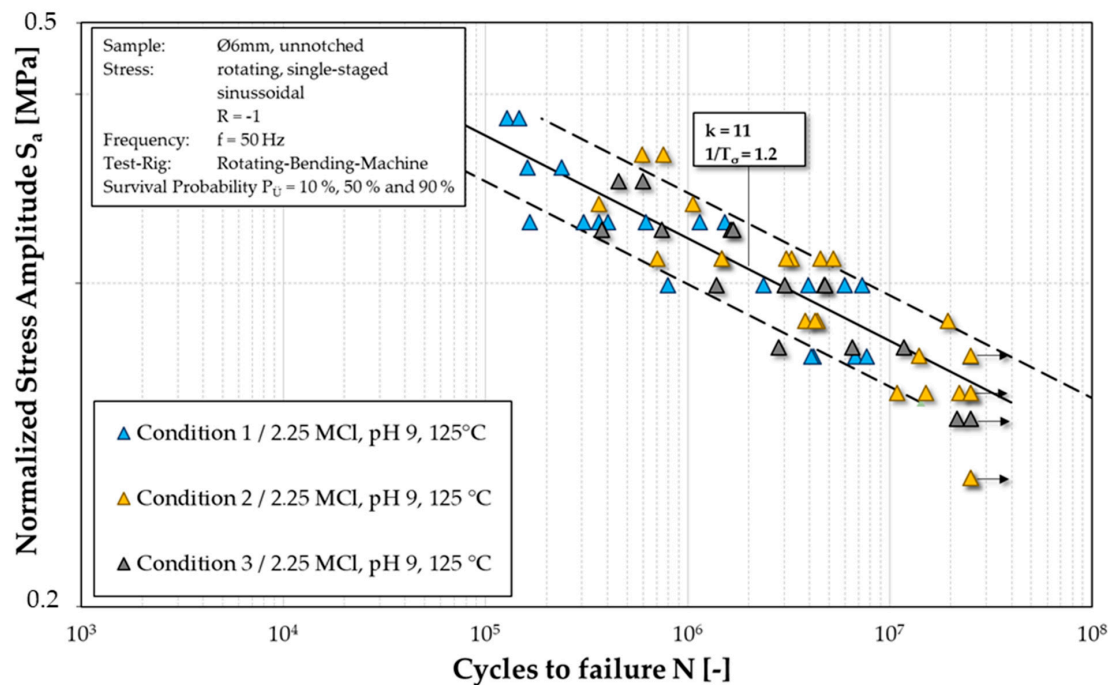


**Figure 4.** Results from the CF tests displayed in a double logarithmic Wöhler diagram. The stress amplitudes are normalized according to the respective tensile strength of the metallurgical condition. S/N curves are calculated with a survival probability of 10%, 50% and 90% respectively.

#### 4. Discussion

The superior fatigue strength observed for condition 3 is assumed to be related to its microstructural particularities. Recently, the amount of  $\gamma'$  in the microstructure of alloy 718 determined by neutron scattering techniques was demonstrated to increase to 19% by the double precipitation-hardening treatment used for producing condition 2, compared to 13% obtained by a single step by 760 °C, both having a similar amount of  $\gamma''$  (14%) [15]. By a slight increase of the ageing temperatures a further increase in the amount of strengthening phases in spite of the reduction of the ageing time is expected to occur. The additional reduction in the content of  $\delta$ -phase is also assumed to have a beneficial impact compared to condition 1. Surprisingly, the lower tensile strength of condition 1 did not have a dominating impact on its fatigue strength. In fact, the fatigue behavior of condition 1 in air was comparable to the one for condition 3 (Figure 3). As stated previously, among all three conditions, condition 1 should contain the largest amount of  $\delta$ -phase in its microstructure. The nucleation of  $\delta$ -phase consumes niobium, which is necessary for the formation of the strengthening  $\gamma''$ -phase. Therefore, the presence of  $\delta$ -phase at the grain boundaries should lead to a lower amount of  $\gamma''$ -phase in adjacent areas, thus increasing the support effect within the plastic zone at the vicinity of the crack tip. This could positively influence the fatigue strength of the material by increasing the ductility of these adjacent areas.

On the other hand, the largest reduction in fatigue strength was determined for condition 1 when exposed to the brine at 125 °C. This could be explained by the presence of  $\delta$ -phase at the grain boundaries, because  $\delta$ -phase is well known for having a detrimental effect on the cracking resistance of alloy 718 [14,19]. The results from the cyclic potentiodynamic polarization tests, however, did not support this hypothesis. Electrochemical tests are appropriate to assess the uniform and localized corrosion behavior of metallic materials. In fact, electrochemical techniques have been successfully used in the past to elucidate how pitting resistance affects the CF resistance of stainless steels [20–25]. However, in the present study electrochemical results alone could not be utilized to infer the CF behavior of alloy 718. Since the corrosion behavior of alloy 718 is mainly influenced by inclusions [26,27], and conventional electrochemical techniques do not have enough resolution to assess the influence of these microstructural particularities, the obtained electrochemical results should be taken carefully. Nevertheless, the excellent pitting corrosion resistance of 718 observed during the cyclic potentiodynamic polarization tests correlates well with the absence of pitting determined on the specimens after CF testing. Remarkable is also the excellent CF resistance determined for condition 2, which can be explained by the longer aging times leading to a homogenous distribution of fine  $\gamma'$ - or  $\gamma''$ -precipitates as well as  $\delta$ -phase depletion. This microstructure of alloy 718 has shown indeed a superior resistance to other cracking mechanisms [14,15]. The slightly lower fatigue strength compared to conditions 1 and 3 is compensated by the microstructure leading to an excellent CF behavior.

By normalizing the stress amplitudes using the respective tensile strength of each condition (Figure 4) the influence of the strength-controlling microstructure can be assessed. The normalization led to an overall scatter band ( $1/T_\sigma$ ) of 1.2 for all three conditions, which is within the tolerance for metallic materials in air at room temperature [28]. Considering that Figure 4 includes results obtained in a corrosive environment, the obtained  $1/T_\sigma$  becomes neglectable. The results clearly indicate that microstructural particularities, which defines not only the strength but also the corrosion resistance in alloy 718, play a relevant role in its CF behavior. This contrast with preliminary results, where no significant differences in the corrosion fatigue crack propagation rate in a 3.5 wt % NaCl-solution at 80 °C between two metallurgical conditions of alloy 718 were observed [29]. This disagreement could be attributed to the test environment used in the present study, which contains a higher chloride concentration, and to the higher test temperature. Furthermore, the reduced tensile strength together with the increased ductility characteristic for condition 1 that, as previously discussed, is assumed to be beneficial for its fatigue behavior, becomes no longer relevant for CF. The obtained experimental results also suggest that future heat treatment

development for alloy 718 could be data science-based. This approach should consider the microstructure of the material to optimize its fatigue and CF resistance. However, it has to be considered that the dependency of the CF behavior on the microstructure in alloy 718 shown in this study was drawn from the results obtained only on the three investigated metallurgical conditions. Therefore, it has to be further investigated to what extent it can be extrapolated to other microstructures of alloy 718.

## 5. Conclusions

The following conclusions can be drawn from the experimental results obtained in this study:

1. Electrochemical as well as fatigue and CF examinations were successfully conducted on three different metallurgical conditions of alloy 718. The CF behavior was determined using customized rotating bending machines enabling testing in a simulated drilling environment consisting in a 2.25 mol/L Cl-containing solution of pH 9 at 125 °C.
2. Among all investigated metallurgical conditions of alloy 718, conditions 1 and 3 have shown the largest fatigue strength in air at room temperature. It is assumed that the large amount of the strengthening phases  $\gamma'$  and  $\gamma''$  as well as the refinement of these precipitates confers condition 3 an excellent fatigue behavior. Opposite to conditions 2 and 3, the presence of a limited amount of  $\delta$ -phase at the grain boundaries in condition 1 is expected to enhance the support effect in the plastic zone at the vicinity of the crack tip.
3. While the largest reduction in fatigue strength was determined for condition 1, condition 2 has shown a remarkable CF resistance when exposed to the alkaline 2.25 mol/L Cl-containing brine at 125 °C. This difference cannot be explained only in terms of pitting corrosion susceptibility, because the electrochemical results as well as the appearance of the specimens after testing have confirmed the excellent pitting corrosion resistance of all three investigated metallurgical conditions in the test environment. On the other hand, it was demonstrated that the microstructure of alloy 718 plays a relevant role in its CF behavior. Therefore, the CF behavior of conditions 1 and 2 can be rationalized in terms of their microstructural particularities, in particular, by the presence of  $\delta$ -phase.

**Author Contributions:** Conceptualization, C.T.E. and H.S.K.; methodology, C.T.E. and H.S.K.; validation, C.T.E. and H.S.K.; investigation, C.T.E. and H.S.K.; resources, H.S.K.; data curation, C.T.E. and H.S.K.; writing—original draft preparation, C.T.E. and H.S.K.; writing—review and editing, C.T.E., H.S.K. and M.O.; visualization, C.T.E. and H.S.K.; supervision, H.S.K. and M.O.; project administration, C.T.E. and M.O. All authors have read and agreed to the published version of the manuscript.

**Funding:** This research received no external funding.

**Institutional Review Board Statement:** Not applicable.

**Informed Consent Statement:** Not applicable.

**Data Availability Statement:** Not applicable.

**Acknowledgments:** The authors would like to thank Baker Hughes for enabling the publication of the experimental results.

**Conflicts of Interest:** The authors declare no conflict of interest.

## References

1. Vaisberg, O.; Vincklé, O.; Permin, G.; Sarda, J.P.; Fay, J.B. Fatigue of Drillstring: State of the Art. *Oil Gas Sci. Technol.* **2002**, *57*, 7–37. [[CrossRef](#)]
2. ASME Shale Shaker Committee. *Drilling Fluids Processing Handbook*; Elsevier Science: Amsterdam, The Netherlands, 2004.



3. De Barbadillo, J.J.; Mannan, S.K. Alloy 718 for the Oilfield Applications. In *Superalloy 718 and Derivates*; Ott, E., Groh, J.R., Banik, A., Dempster, I., Gabb, T.P., Helmink, R., Liu, X., Sjöberg, G.P., Wusatowska-Sarnek, A., Eds.; The Minerals, Metals, and Materials Society: Warrendale, PA, USA, 2010; p. 579.
4. Onyewuenyi, O.A. Alloy 718—Alloy Optimization for Applications in Oil and Gas Production. In *Superalloy 718—Metallurgy and Applications*; Loria, E.A., Ed.; The Minerals, Metals, and Materials Society: Warrendale, PA, USA, 1989; p. 345.
5. Kolts, J. Alloy 718 for the Oil and Gas Industry. In *Superalloy 718—Metallurgy and Applications*; Loria, E.A., Ed.; The Minerals, Metals, and Materials Society: Warrendale, PA, USA, 1989; p. 739.
6. Bhavsar, R.B.; Collins, A.; Silverman, S. Use of Alloy 718 and 725 in Oil and Gas Industry. In *Superalloys 718, 625, 706 and Various Derivates*; Loria, E.A., Ed.; The Minerals, Metals, and Materials Society: Warrendale, PA, USA, 2001; p. 47.
7. De Barbadillo, J.J.; Mannan, S.K. Alloy 718 for Oilfield Applications. *JOM* **2012**, *64*, 265–270. [\[CrossRef\]](#)
8. Badrak, J.P. Status of Precipitation Harneded Nickel Base Alloys Including 718 for Oilfield Applications. In *Superalloy 718 and Derivatives*; Ott, E., Banik, A., Andersson, J., Dempster, I., Gabb, T.P., Groh, J.R., Heck, K., Helmink, R., Liu, X., Wusatowska-Sarnek, A., Eds.; The Minerals, Metals, and Materials Society: Warrendale, PA, USA, 2014; p. 493.
9. Loria, E.A. The Status and Prospects of Alloy 718. *JOM* **1988**, *40*, 36–47. [\[CrossRef\]](#)
10. Schafrik, R.E.; Ward, D.D.; Groh, J.R. Application of Alloy 718 in GE Aircraft Engines: Past, Present and Next Five Years. In *Superalloys, 718, 625, 706 and Various Derivates*; Loria, E.A., Ed.; The Minerals, Metals, and Materials Society: Warrendale, PA, USA, 2001; p. 1.
11. Patel, S.; de Barbadillo, J.; Coryell, S. Superalloy 718: Evolution of the Alloy from High to Low Temperature Application. In *Superalloy 718 and Derivatives*; Ott, E., Banik, A., Andersson, J., Dempster, I., Gabb, T.P., Groh, J.R., Heck, K., Helmink, R., Liu, X., Wusatowska-Sarnek, A., Eds.; The Minerals, Metals, and Materials Society: Warrendale, PA, USA, 2018; p. 23.
12. API Standard 6ACRA. *Age-Hardened Nickel-Based Alloys for Oil and Gas Drilling and Production Equipment*; American Petroleum Institute: Washington, DC, USA, 2015.
13. Aghajani, A.; Tewes, J.; Parsa, A.B.; Hoffmann, T.; Kostka, A.; Kloewer, J. Identification of Mo-Rich  $M_{23}C_6$  Carbides in Alloy 718. *Metall. Mater. Trans. A* **2016**, *47*, 4382–4392. [\[CrossRef\]](#)
14. Klapper, H.S.; Kloewer, J.; Gosheva, O. Hydrogen embrittlement: The game changing Factor in the Applicability of Nickel alloys in Oilfield Technology. *Phil. Trans. R. Soc. A* **2017**, *375*, 20160415. [\[CrossRef\]](#) [\[PubMed\]](#)
15. Botinha, J.; Alves, H.; Gehrman, B.; Gilles, R.; Solis, C.; Munke, J.; Feoktystov, A.; Baran, V. Study of Phase Distribution on Alloy UNS N07718 in Different Hardening Conditions and its Relationship with Hydrogen Embrittlement Susceptibility. In Proceedings of the NACE Corrosion Conference 2019, New Orleans, LA, USA, 24–28 March 2019; NACE International: Houston, TX, USA, 2019; Paper no. C2019-13025.
16. Klapper, H.S.; Stevens, J. Susceptibility to Pitting Corrosion of Nickel-Based Alloy 718 exposed to Simulated Drilling Environments. *Corrosion* **2014**, *70*, 899–906. [\[CrossRef\]](#)
17. Engler, C.T.; Andersohn, G.; Oechsner, M.; Sarmiento Klapper, H.; Stevens, J. Understanding and addressing the challenges of assessing the corrosion fatigue of metallic materials for drilling applications. In Proceedings of the NACE Corrosion Conference 2019, New Orleans, LA, USA, 24–28 March 2019; NACE International: Houston, TX, USA, 2019. Paper No 8918.
18. Klapper, H.S.; Rebak, R.B. Assessing the Pitting Corrosion Resistance of Oilfield Nickel Alloys at Elevated Temperatures by Electrochemical Methods. *Corrosion* **2017**, *73*, 666–673. [\[CrossRef\]](#)
19. Miglin, M.T.; Nelson, J.L. Strain Rate Sensitivity of Alloy 718 Stress Corrosion Cracking. In *Superalloys 718, 625 and Various Derivatives*; Loria, E.A., Ed.; The Minerals, Metals, and Materials Society: Warrendale, PA, USA, 1991; pp. 695–704.
20. Sonnleitner, R.; Mori, G.; Panzenboeck, M.; Fluch, R.; Eglsäer, S. Corrosion Fatigue of a CrMnN Stainless Steel. In Proceedings of the NACE Corrosion Conference 2008, New Orleans, LA, USA, 16–20 March 2008; NACE International: Houston, TX, USA, 2008; Paper no. C2008-08488.
21. Vichytil, C.; Sonnleitner, R.; Mori, G.; Panzenboeck, M.; Fluch, R. Corrosion Fatigue Investigations on Austenitic Stainless Steels with Different Alloying Concepts. In Proceedings of the NACE Corrosion Conference 2010, San Antonio, TX, USA, 14–18 March 2010; NACE International: Houston, TX, USA, 2010; Paper no. C2010-10302.
22. Vichytil, C.; Sonnleitner, R.; Mori, G.; Panzenboeck, M.; Fluch, R. Corrosion Fatigue Investigations of CrNiMoN Austenitic Stainless Steels. In Proceedings of the NACE Corrosion Conference 2011, Houston, TX, USA, 13–17 March 2011; NACE International: Houston, TX, USA, 2011; Paper no. C2011-11297.
23. Chen, W.; Klapper, H.S.; Stevens, J. Effects of Pitting and Inclusions on the Corrosion Fatigue of a CrMnN Stainless Steel. In Proceedings of the NACE Corrosion Conference 2014, San Antonio, TX, USA, 9–13 March 2014; NACE International: Houston, TX, USA, 2014; Paper no. C2014-04070.
24. Visser, A.; Mori, G.; Pippan, R.; Kapp, M.; Fluch, R.; Panzenboeck, M.; Holper, B. Influence of Different Types of Localized Corrosion on the Fatigue Behavior of an Austenitic Stainless Steel. In Proceedings of the NACE Corrosion Conference 2016, Vancouver, BC, Canada, 6–10 March 2016; NACE International: Houston, TX, USA, 2016; Paper no. C2016-07599.
25. Klapper, H.S.; Menendez, C.; Jesse, S. Pitting Corrosion Resistance Influencing Corrosion Fatigue Behavior of an Austenitic Stainless Steel in Chloride-Containing Environments. *Corrosion* **2020**, *76*, 398–410. [\[CrossRef\]](#)
26. Garfias-Mesias, L.F.; Klapper, H.S.; Kloewer, J.; Botinha, J. Determination of Precursor Sites for Pitting Corrosion of UNS N07718 in Chloride Environments—Part 2. In Proceedings of the NACE Corrosion Conference 2018, Phoenix, AZ, USA, 15–19 April 2018; NACE International: Houston, TX, USA, 2018; Paper no. C2018-11387.

- 
27. Alekseeva, E.; Karasev, A.; Jönsson, P.G.; Alkhimenko, A. Effect of Inclusions on the Corrosion Properties of the Nickle-Based Alloys 718 and EP718. *Metals* **2020**, *10*, 1177. [[CrossRef](#)]
  28. Radaj, D.; Vormwald, M.E. *Advanced Methods of Fatigue Assessment*, 3rd ed.; Springer: Berlin, Germany, 2007.
  29. Chen, T.; Nutter, J.; Bai, J.; Hawk, J.; Liu, X. Corrosion Fatigue Crack Growth Behavior of Oil-grade Nickel-base alloy 718. Part 2: Effect of Aging Treatment. *Corros. Sci.* **2015**, *98*, 280–290. [[CrossRef](#)]